Calculation of Ferrite Core Losses with Arbitrary Waveforms using the Composite Waveform Hypothesis

Thomas Guillod*, Jenna S. Lee*, Haoran Li†, Shukai Wang†, Minjie Chen†, and Charles R. Sullivan*

*Dartmouth College, Hanover NH, United States
†Princeton University, Princeton NJ, United States

***Abstract*—A method, the improved generalized composite calculation (iGCC) is proposed for computing ferrite core losses. This method, which is an extension of the well-known improved generalized Steinmetz equation (iGSE), applies the composite waveform hypothesis (CWH) to arbitrary excitations by using a time-varying local equivalent frequency that describes the rate of change of the magnetic flux density. The advantages of the proposed method include the ability to model materials in a wide frequency range, especially waveforms with extreme duty cycles. Measurements conducted with "EPCOS TDK N87" ferrite material (with triangular and trapezoidal excitations, across a range of temperatures) show a significant improvement over the state-of-the-art.**

***Index Terms*—Magnetic materials, ferrites, magnetic hysteresis, magnetic losses, core losses, modeling, composite waveform hypothesis, iGSE, iGCC.**

I. Introduction

Accurate prediction of losses in magnetic materials is a longstanding challenge for magnetics design in power electronics [1]–[3]. The loss phenomena are complex and nonlinear, and although the fundamental physical phenomena giving rise to loss are understood, the physical understanding is not sufficient to accurately predict loss in the situations of interest. Hence, semi-empirical loss prediction methods are necessary [4]–[9]. This is difficult because the loss generally depends on the frequency, amplitude, waveform, and dc bias of the exciting waveform, as well as the specific magnetic material, the core geometry, and the temperature of the core.

Even just considering the effect of the waveform, the challenges are complex. Multiple methods have been proposed to use limited data to predict losses for a wider variety of waveforms [4]–[6], [8], [10]. The most popular of these is the *improved generalized Steinmetz equation* (iGSE) [6], [11]. Its accuracy is limited, but it has the advantage that it can be applied to any flux waveform, and the required parameters can be derived from readily available loss data. The iGSE can be written in terms of an integral for any general waveform, or, for a piecewise linear waveform, it can be written as a sum of the loss associated with each segment.

The concept that the core loss can be written as the sum of the loss associated with each segment of a waveform is termed the *composite waveform hypothesis* (CWH) and can provide an intuitive understanding of the loss behavior of soft-magnetic materials [12]. Many loss calculation methods, including the iGSE, implicitly or explicitly rely on the CWH. Unfortunately, the CWH does not strictly hold true; the main limitation being the exclusion of the *relaxation effects* [10], [12]. Nonetheless, loss predictions based on the CWH have shown to provide useful accuracy in practice for both triangular and trapezoidal waveforms [12].

In [13], the *improved Steinmetz equation* (ISE), which is directly based on the CWH, was demonstrated to be more accurate than the iGSE, albeit only for triangular waveforms. Although the ISE offers better accuracy than the iGSE for triangular waveforms, it also loses the full generality of the iGSE. In this paper, we introduce an approach, the *improved generalized composite calculation* (iGCC), that combines the improved triangle-wave accuracy of the ISE with the ability of the iGSE to deal with arbitrary waveforms, while also simplifying the formulation relative to the ISE, making it practical for designers to apply. In fact, the iGSE is a special case of the iGCC and, therefore, the iGCC can be considered as an extension of the iGSE.

This paper is organized as follows. Section II reviews state-of-the-art loss equations for arbitrary waveforms. Section III details the CWH for triangular waveforms and introduces the iGCC for arbitrary waveforms. Section IV describes the parametrization of the model and experimentally verifies the iGCC with measurements conducted with "EPCOS TDK N87". Section V analyses the impact of the temperature on the performance of the iGCC and, finally, Section VI highlights the impact of the magnetic relaxation on the losses.

II. State-of-the-art Loss Equations

This section reviews three existing loss equations applicable to arbitrary waveforms. These state-of-the-art methods will be used as a benchmark for the proposed loss equation. The first method is the widely used iGSE, which is described by the following integral [6]:

$$P = \frac{1}{T} \int_0^T k \left| \frac{\mathrm{d}B}{\mathrm{d}t} \right|^{\alpha} \left(B_{\mathrm{pkpk}}\right)^{\beta-\alpha} \mathrm{d}t, \tag{1}$$

where T is the waveform period, B the flux density, and B_{pkpk} the peak-to-peak flux density. The Steinmetz parameters k, α, and β are empirical quantities that are extracted from measurements and/or from the material datasheet. The Steinmetz parameters are typically computed with a least squares fit from sinusoidal or symmetric triangular ($50\,\%$ duty cycle) data.

More recently, an alternative loss equation, relying on the second derivative of the magnetic flux density and Steinmetz parameters, has been proposed [8], [14]:

$$P = k f \left(f_{\mathrm{eq}}\right)^{\alpha-1} B_{\mathrm{pkpk}}^{\beta}, \tag{2}$$

$$f_{\mathrm{eq}} = \frac{1}{4\pi B_{\mathrm{pkpk}}} \int_0^T \left| \frac{\mathrm{d}^2 B}{\mathrm{d}t^2} \right| \mathrm{d}t, \tag{3}$$

where T is the waveform period, f the frequency, B the flux density, and B_{pkpk} the peak-to-peak flux density. Similarly to the iGSE, the Steinmetz parameters can be fitted with sinusoidal or symmetric triangular (50 % duty cycle) data. In this paper, this loss equation will be referred as the *Stenglein Steinmetz loss equation* (SSLE).

In [8], [14], [15], another version of the SSLE is also introduced. The losses are described as the quasi-static hysteresis losses (W_{hyst}) multiplied by an effective frequency (f_{eff}), which is dependent on the second derivative on the magnetic flux density:

$$P = W_{\mathrm{hyst}} f_{\mathrm{eff}}, \tag{4}$$

$$W_{\mathrm{hyst}} = a_1 B_{\mathrm{pkpk}} + a_2 B_{\mathrm{pkpk}}^2 + a_3 B_{\mathrm{pkpk}}^3, \tag{5}$$

$$f_{\mathrm{eff}} = f \left(1 + c \left(\frac{1}{B_{\mathrm{pkpk}}} \int_0^T \left| \frac{\mathrm{d}^2 B}{\mathrm{d}t^2} \right| \mathrm{d}t \right)^{\gamma} \right), \tag{6}$$

where T is the waveform period, f the frequency, B the flux density, and B_{pkpk} the peak-to-peak flux density. The coefficients a_i are fitted with the quasi-static hysteresis losses. The frequency and waveform dependencies of the core losses are described with the empirical parameters c and γ which are fitted with sinusoidal or symmetric triangular (50 % duty cycle) data. In this paper, this loss equation will be referred as the *Stenglein effective frequency loss equation* (SEFLE).

It should be noted that none of the aforementioned equations (iGSE, SSLE, and SEFLE) consider relaxation losses [10], [12]. The impact of DC bias on the losses can be included but is outside the scope of this paper [8], [16]. Waveforms with minor hysteresis loop can be handled with minor loop decomposition as explained in [6], [17]. If the considered waveform is piecewise linear, the iGSE integral can be reduced to a summation over the different segments. For the SSLE and SEFLE, the second derivative of a piecewise linear waveform consists of Dirac delta pulses and, therefore, the integral can also be transformed into a simple summation.

III. Improved Generalized Composite Calculation

This section reviews the usage of the CWH with a loss map for computing the losses associated with triangular waveforms, as shown in [12]. Afterward, the iGCC, which is applicable to arbitrary waveforms, is introduced.

A. CWH for Triangular Waveforms

Under the CWH, we can find the loss of an asymmetric triangular waveform by decomposing it into two symmetric triangular waveforms with the same slew rates and amplitudes, as shown in Fig. 1 [12]. The frequency of the symmetric triangular waveforms can be calculated as

$$f_1 = \frac{1}{2}\frac{f}{D}, \qquad f_2 = \frac{1}{2}\frac{f}{1-D}, \tag{7}$$

where f is the fundamental frequency, D the duty cycle, and f_1 and f_2 the frequencies of the symmetric waveforms. The energy loss of the rising and falling edges is defined as half of the energy of the symmetric waveforms:

$$W_1 = \frac{P_{\mathrm{sym}}\left(f_1, B_{\mathrm{pkpk}}\right)}{2 f_1}, \quad W_2 = \frac{P_{\mathrm{sym}}\left(f_2, B_{\mathrm{pkpk}}\right)}{2 f_2}. \tag{8}$$

where B_{pkpk} is the peak-to-peak flux density. The function $P_{\mathrm{sym}}\left(f, B_{\mathrm{pkpk}}\right)$ returns the loss density for a symmetric triangular waveform for a given frequency and amplitude (loss map). Under the CWH, the energy loss of the rising and falling edges can be added, and the loss density of the asymmetric waveform can be expressed as

$$P = f\left(W_1 + W_2\right). \tag{9}$$

Alternatively, the loss map $P_{\mathrm{sym}}\left(f, B_{\mathrm{pkpk}}\right)$ can be expressed with frequency-dependent Steinmetz parameters. This is the concept of the ISE loss model presented in [13].

B. iGCC with a Loss Map

The CWH-based methods (loss map and ISE) proposed in [12], [13] are limited to triangular and trapezoidal waveforms. In this paper, an extension is proposed for arbitrary periodic waveforms. First, a time-varying *local equivalent frequency* is

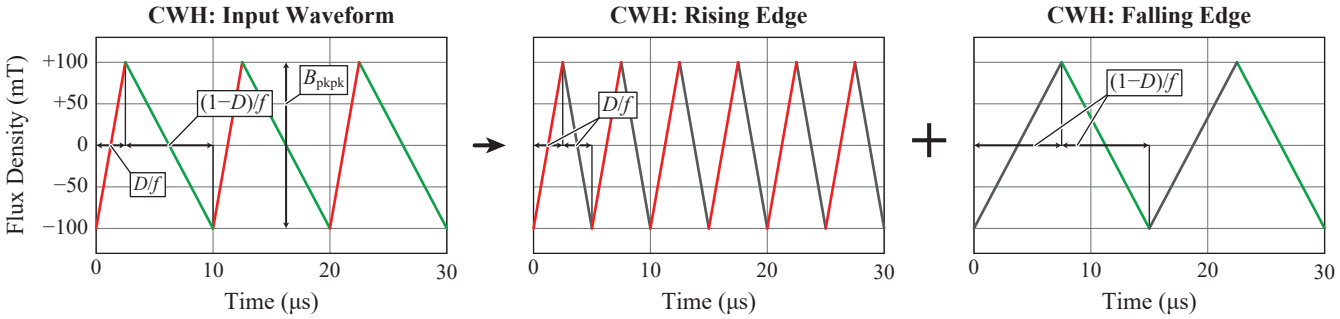

Fig. 1. CWH for an asymmetric triangular waveform. The input excitation is decomposed into two symmetric triangular waveforms with different frequencies. The input waveform has the following parameters: $f = 100\,\mathrm{kHz}$, $D = 25\,\%$, and $B_{\mathrm{pkpk}} = 200\,\mathrm{mT}$.

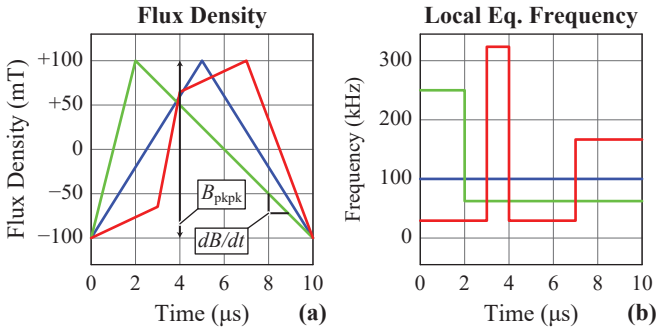

Fig. 2. Illustration of the local equivalent frequency for arbitrary waveforms. (a) Piecewise linear waveforms. (b) Local equivalent frequencies. The input waveforms have the following parameters: $f = 100\,\text{kHz}$ and $B_{\text{pkpk}} = 200\,\text{mT}$.

introduced and quantifies the instantaneous rate of change of the magnetic flux density:

$$\widetilde{f}(t) = \frac{1}{2}\frac{\left|\frac{\mathrm{d}B}{\mathrm{d}t}\right|}{B_{\text{pkpk}}}. \tag{10}$$

As shown in Fig. 2, each segment of a piecewise linear waveform has an equivalent frequency. For triangular waveforms, the time-varying local frequency is equivalent to the frequencies defined in (7). The local equivalent frequency has the following property for waveforms without minor loops (or after minor loop splitting) [6]:

$$\int_0^T \widetilde{f}(t)\,\mathrm{d}t = 1. \tag{11}$$

With the time-varying local equivalent frequency, an arbitrary waveform can be decomposed into many symmetric triangular waveforms and the loss density can be computed with the CWH. The resulting loss model, the iGCC, is expressed as

$$P = \frac{1}{T}\int_0^T P_{\text{sym}}\left(\widetilde{f}(t), B_{\text{pkpk}}\right)\mathrm{d}t. \tag{12}$$

The iGCC states that the loss density of an arbitrary waveform can be approximated by averaging the loss density of the symmetric triangular waveforms defined by the local equivalent frequency. The iGCC offers an intuitive qualitative and quantitative understanding of the impact of fast transient on the core losses.

For piecewise linear waveforms, the integral can be reduced to a summation. A piecewise linear waveform with n intervals consists of $n+1$ sample points, and can be described as:

$$\Delta B_i = B_i - B_{i-1}, \tag{13}$$

$$\Delta t_i = t_i - t_{i-1}, \tag{14}$$

$$f = \frac{1}{t_n - t_0}, \tag{15}$$

where $\{B_0, \ldots, B_n\}$ and $\{t_0, \ldots, t_n\}$ are the sample points. The waveform is periodic ($B_0 = B_n$). In this case, the iGCC can be reformulated as

$$P = f\sum_{i=1}^{n} P_{\text{sym}}\left(\frac{1}{2}\frac{\left|\frac{\Delta B_i}{\Delta t_i}\right|}{B_{\text{pkpk}}}, B_{\text{pkpk}}\right)\Delta t_i. \tag{16}$$

C. iGCC with a Steinmetz Fit

The iGCC can be directly used to compute core losses if a loss map and/or an interpolant is available for $P_{\text{sym}}(f, B_{\text{pkpk}})$. Alternatively, the losses associated with symmetric triangular waveforms can be described with frequency-dependent Steinmetz parameters:

$$P_{\text{sym}}(f, B_{\text{pkpk}}) = \lambda(f)\, B_{\text{pkpk}}^{\beta(f)}. \tag{17}$$

where $\lambda(f)$ and $\beta(f)$ are extracted with symmetric triangular data. With the Steinmetz fit, the iGCC can be formulated as:

$$P = \frac{1}{T}\int_0^T \lambda\left(\widetilde{f}(t)\right) B_{\text{pkpk}}^{\beta\left(\widetilde{f}(t)\right)}\,\mathrm{d}t. \tag{18}$$

It should be noted that, unlike other methods, the iGCC does not require the Steinmetz frequency exponent α (see (17)). This is an advantage as the extraction of the exponent α is very sensitive to measurement noise and uncertainties [18].

D. Link between the iGCC and the iGSE

The iGCC is closely related to the well-known iGSE. In order to highlight the relation, the following function $P_{\text{sym}}(f, B_{\text{pkpk}})$ is selected:

$$P_{\text{sym}}(f, B_{\text{pkpk}}) = k\,(2f)^{\alpha}\, B_{\text{pkpk}}^{\beta}, \tag{19}$$

where k, α, and β are constant (frequency-independent) Steinmetz parameters. The resulting loss equation is obtained by the combination of (10), (12), and (19):

$$P = \frac{1}{T}\int_0^T k\left(2\frac{1}{2}\frac{\left|\frac{\mathrm{d}B}{\mathrm{d}t}\right|}{B_{\text{pkpk}}}\right)^{\alpha} B_{\text{pkpk}}^{\beta}\,\mathrm{d}t. \tag{20}$$

This last equation is equivalent to the iGSE (see (1)). Hence, the iGSE is a special case of the iGCC. The main advantage of the iGCC is the ability to model a complex surface for $P_{\text{sym}}(f, B_{\text{pkpk}})$ whereas the iGSE is limited to a plane (in logarithmic scales; see (19)).

IV. Experimental Validation

In this section, the proposed iGCC and the reviewed state-of-the-art methods (iGSE, SSLE, and SEFLE) are experimentally verified for "EPCOS TDK N87" ferrite material.

A. Core Material and Operating Conditions

The "EPCOS TDK N87" ferrite material, which is one of the most commonly used ferrites for power electronic systems, has been selected for the experimental validation of the iGCC [19]. The measurements are conducted on a "R22.1X13.7X7.9" toroid and the following operating conditions were measured: $f \in [50, 500]\,\text{kHz}$, $B_{\text{pkpk}} \in [50, 600]\,\text{mT}$, $P > 5\,\text{mW/cm}^3$, and $T = 25\,^{\circ}\text{C}$. The dataset consists of 815 symmetric triangular waveforms (i.e. waveshapes with two linear segments having the same slope), 2456 asymmetric triangular waveforms (i.e. waveshapes with two linear segments having different slopes), and 1449 asymmetric trapezoidal waveforms (i.e. waveshapes with four linear segments having non-zero slopes). As shown in Fig. 3, the duty cycle of the different segments is always larger than 10 % and smaller than 90 %. The dataset is

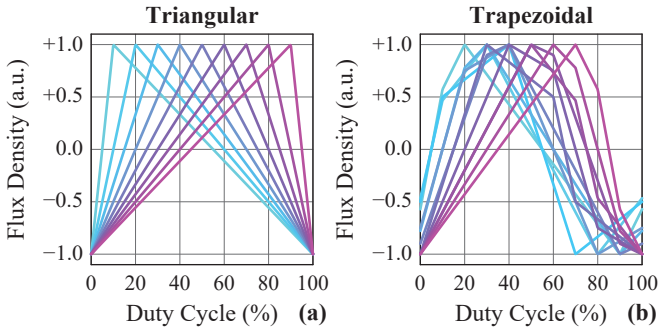

Fig. 3. (a) Triangular and (b) trapezoidal waveshapes contained in the dataset. The duty cycle of the different segments is swept with 10 % steps. For the trapezoidal waveshapes, excitations with constant flux density segments are excluded.

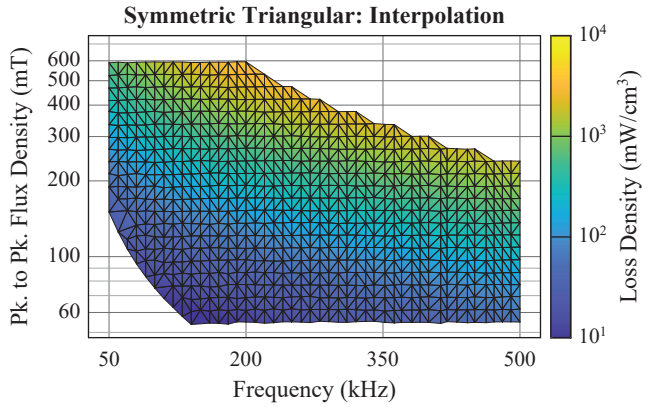

Fig. 4. Delaunay triangulation and interpolation between the symmetric triangular waveforms. A linear interpolant is used with a logarithmic transformation of all the variables.

part of the MagNet initiative [20], [21] and is openly available (see Appendix).

B. Model Parametrization

The 815 symmetric triangular waveforms are used to parametrize the different equations. For the iGSE (see (1)), SSLE (see (2)), and SEFLE (see (4)), the parameters are extracted with a least squares fit with respect to the relative error on the core losses [22]. For the iGCC, two different variants of the method are used:

- $\text{iGCC}_{\text{fit.}}$ - see Section III-B - A Delaunay triangulation between the different symmetric triangular waveforms is created and the loss density is linearly interpolated on the triangulation (in a logarithmic scale) [23]. Fig. 4 depicts the triangulation and the interpolated data.
- $\text{iGCC}_{\text{int.}}$ - see Section III-C - The Steinmetz parameters are extracted from the symmetric triangular waveforms with a least-squares regression for each frequency present in the dataset [22]. The obtained parameters ($\lambda(f)$ and $\beta(f)$) are then fitted with a third-degree polynomial expression in order to obtain a simple analytical expression and remove the noise. Figs. 5(a)-(b) shows the extracted parameters and the corresponding cubic fits. Fig. 5(c) shows the accuracy of the fit for symmetric triangular waveforms. The deviation between the measurement and the Steinmetz fit is below 10 % over the complete range.

TABLE I
ERROR METRICS / SYM. TRIANGULAR WAVEFORMS.

Model	Avg.	RMS	95$^{\text{th}}$ pct.	Max.
iGSE	7.7 %	9.1 %	16.4 %	20.6 %
SSLE	7.7 %	9.1 %	16.4 %	20.6 %
SEFLE	3.2 %	3.7 %	5.9 %	9.1 %
$\text{iGCC}_{\text{fit.}}$	2.4 %	3.0 %	6.0 %	10.6 %
$\text{iGCC}_{\text{int.}}$	0.0 %	0.0 %	0.0 %	0.0 %

Table I depicts error metrics (average, RMS, 95$^{\text{th}}$ percentile, and maximum) of the absolute relative error between the fitted models and the 815 measured symmetric triangular waveforms. The iGSE and the SSLE are equivalent for symmetric triangular waveforms and, therefore, feature the same error metrics. The additional degrees of freedom offered by the SEFLE and $\text{iGCC}_{\text{fit.}}$ allows for a better fitting of the symmetric triangular

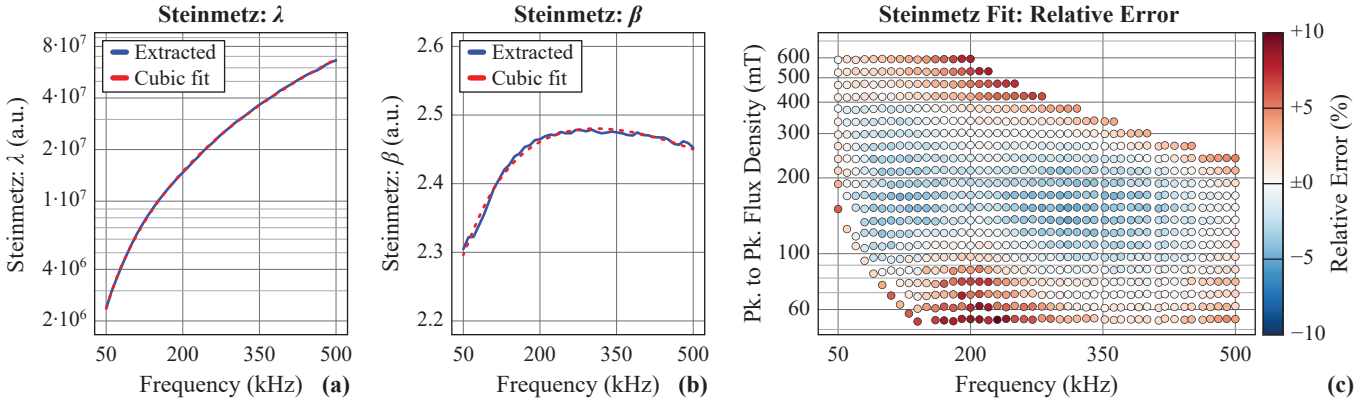

Fig. 5. (a)-(b) Steinmetz parameters (17) extracted from the symmetric triangular waveforms. The parameters λ and β are scaled such that $[P] = \text{W/m}^3$. (c) Accuracy of the fit for symmetric triangular waveforms.

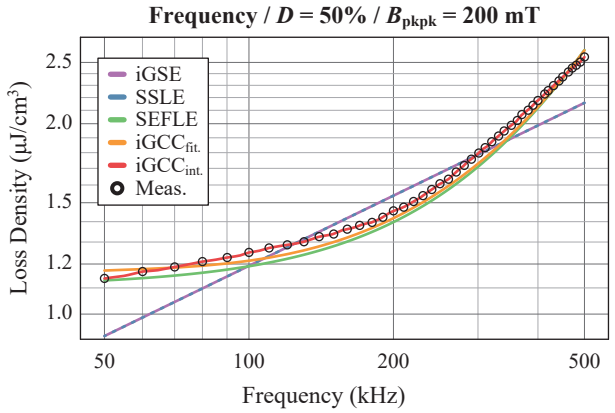

Fig. 6. Energy loss density (per cycle) for symmetric triangular waveforms at different frequencies ($f \in [50, 500]$ kHz, $D = 50\,\%$, and $B_{\mathrm{pkpk}} = 200\,\mathrm{mT}$). The iGSE, SSLE, SEFLE, and iGCC are compared to measurements.

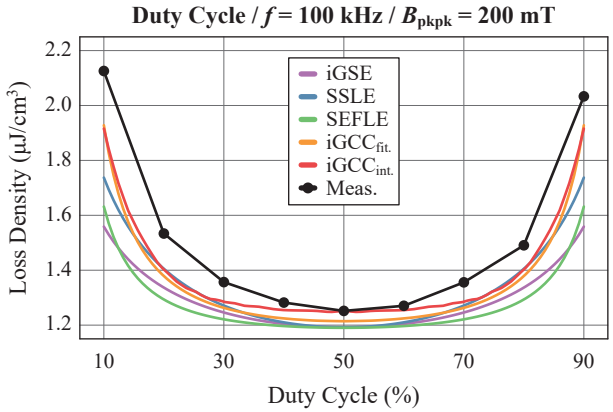

Fig. 7. Energy loss density (per cycle) for triangular waveforms with different duty cycles at a constant frequency and flux density ($D \in [10, 90]\,\%$, $f = 100\,\mathrm{kHz}$, and $B_{\mathrm{pkpk}} = 200\,\mathrm{mT}$). The iGSE, SSLE, SEFLE, and iGCC are compared to measurements.

waveforms. Finally, the error is zero for the iGCC$_{\mathrm{int.}}$ as the measured waveforms are directly used for the interpolation.

It should be noted that, for some asymmetric triangular and trapezoidal waveforms, the iGCC needs to evaluate $P_{\mathrm{sym}}\left(f, B_{\mathrm{pkpk}}\right)$ outside the measured range (see (10), (12), and Fig. 4). In this paper, the dataset has been curated to exclude such waveforms. Another solution would be to extrapolate the data which is always difficult for core materials. The fact that the iGCC requires measured loss data for a large range of symmetric triangular waveforms represents a limitation of the method. However, it should be noted that other methods (such as the iGSE, SSLE, and SEFLE) are, to some extent, subject to the same issue as the material behavior is also implicitly extrapolated outside the fitting range.

C. Loss Prediction

Fig. 6 shows the energy loss density (per cycle) for symmetric triangular waveforms at different frequencies. The use of constant Steinmetz parameters for the iGSE and SSLE implies that the relation between the losses and the frequency is linear (in a logarithmic scale), which explains why the iGSE and SSLE are not able to capture the material behavior over a wide frequency range. In contrast, the SEFLE and iGCC$_{\mathrm{fit.}}$ allow for the description of the core loss characteristics over a wide frequency range. The iGCC$_{\mathrm{int.}}$ is, per definition, perfectly fitting in the complete frequency range for symmetric triangular waveforms.

Fig. 7 shows the energy loss density (per cycle) for triangular waveforms with different duty cycles. It can be seen that the iGCC performs better than the iGSE, SSLE, and SEFLE for waveforms with extreme duty cycles. This can be explained by the usage of the local equivalent frequency (10) in the iGCC that explicitly takes into account the fast transients occurring with extreme duty cycles, whereas the iGSE uses the same set of Steinmetz parameters for every transient. However, it should be noted that all methods still underestimate the losses, which could be explained by relaxation losses (not included in the considered models). Relaxation losses not only affect waveforms including constant flux density intervals but also waveforms combining fast and slow transients, e.g., triangular excitations with extreme duty cycles.

TABLE II
ERROR METRICS / ALL WAVEFORMS.

Model	Avg.	RMS	95$^{\mathrm{th}}$ pct.	Max.
iGSE	7.5 %	9.0 %	16.2 %	27.7 %
SSLE	6.0 %	7.4 %	14.3 %	20.8 %
SEFLE	5.4 %	6.6 %	12.4 %	26.1 %
iGCC$_{\mathrm{fit.}}$	4.7 %	5.9 %	11.9 %	16.9 %
iGCC$_{\mathrm{int.}}$	3.3 %	4.8 %	11.1 %	16.9 %

In order the assess the performance of the different models over a wide range of operating conditions, the relative error between the models and the measurements is computed for the complete dataset (815 symmetric triangular waveforms, 2456 asymmetric triangular waveforms, and 1449 asymmetric trapezoidal waveforms). Fig. 8 depicts the relative error distribution for the different models. Table II shows error metrics (average, RMS, 95$^{\mathrm{th}}$ percentile, and maximum) for the absolute relative error between the models and the measurements. It can be concluded that for "EPCOS TDK N87" at $T = 25\,^{\circ}\mathrm{C}$, the iGCC, with a 95$^{\mathrm{th}}$ percentile error below $12\,\%$, outperforms the iGSE, SSLE, and SEFLE.

The deviation between the iGCC$_{\mathrm{fit.}}$ and iGCC$_{\mathrm{int.}}$ originates from the simplified Steinmetz fit (see Fig. 5) compared to the interpolated data (see Fig. 4). Nevertheless, the error metrics for the iGCC$_{\mathrm{fit.}}$ and iGCC$_{\mathrm{int.}}$ are extremely similar, indicating that the interpolation (see (12)) can be replaced by a simple fit (see (18)) without a significant impact on the accuracy.

V. Impact of Temperature

Most ferrite material behaviors are massively temperature-dependent, including the selected "EPCOS TDK N87" material [2], [19]. For this reason, a dataset including the temperature dependencies of "EPCOS TDK N87" is selected in this section

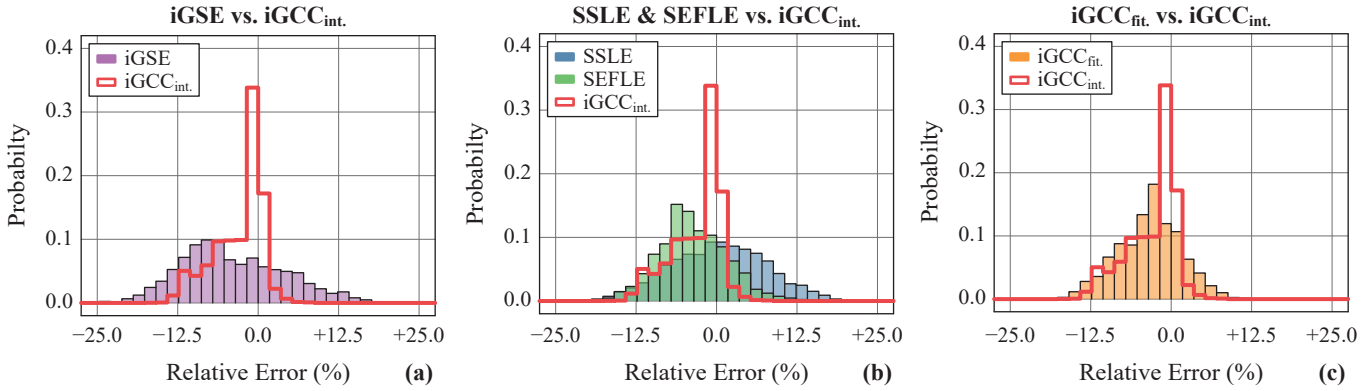

Fig. 8. Distribution of the relative error on the core losses for (a) the iGSE, (b) the SSLE and SEFLE, and (c) the iGCC$_{fit.}$. The best method, the iGCC$_{int.}$ is depicted in each subplot as a comparison. The dataset consists of 815 symmetric triangular waveforms, 2456 asymmetric triangular waveforms, and 1449 asymmetric trapezoidal waveforms.

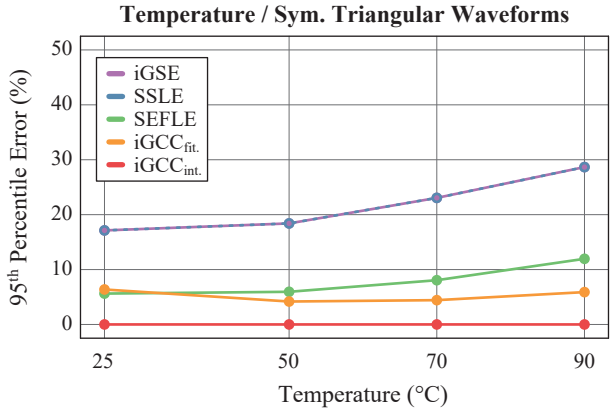

Fig. 9. 95th percentile of the absolute relative error between the fitted models and the measured symmetric triangular waveforms, which describes the ability of the models to fit such waveforms.

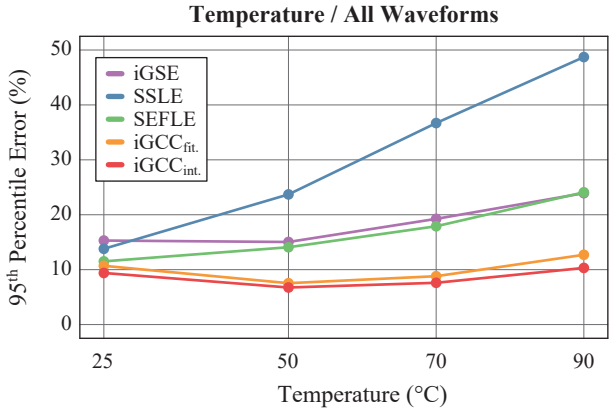

Fig. 10. 95th percentile of the absolute relative error between the models and the measured waveforms (symmetric triangular, asymmetric triangular, and asymmetric trapezoidal), which describes the ability of the models to predict core losses.

(measured on a "R34.0X20.5X12.5" toroid). The following operating conditions are considered: $f \in [50, 500]\,\mathrm{kHz}$, $B_{\mathrm{pkpk}} \in [50, 600]\,\mathrm{mT}$, $P > 5\,\mathrm{mW/cm^3}$, and $T \in \{25, 50, 70, 90\}\,^{\circ}\mathrm{C}$. The dataset consists of 1354 symmetric triangular waveforms, 4306 asymmetric triangular waveforms, and 2863 asymmetric trapezoidal waveforms. The dataset is part of the MagNet initiative [20], [21] and is openly available (see Appendix).

For each temperature, the different models are parametrized with the symmetric triangular waveforms as shown in Section IV-B. Fig. 9 shows the resulting 95th percentile of the absolute relative error between the fitted models and the measured symmetric triangular waveforms. It can be seen that for the iGSE and SSLE, the quality of the fit deteriorates at higher temperatures, meaning that constant Steinmetz parameters are not able to describe the material behavior.

Fig. 10 depicts the 95th percentile of the absolute relative error between the models and the measurements for the complete dataset. The iGCC is clearly the best model and the 95th percentile error is nearly temperature-independent and consistently below 13 %. The SEFLE and the iGSE feature similar performance with a slightly increased error above 70 °C, which can be related to the quality of the parametrization (see Fig. 9). The performance of the SSLE is massively degrading above 50 °C. This is explained by the increased value of the Steinmetz parameter α (see (2)) at higher temperatures. Therefore, for trapezoidal waveforms, small changes of the derivative of the flux density are creating large Dirac delta spikes for the second derivative (see (3)), which combined with a large value of α, are leading to an overestimation of the losses.

VI. Impact of Magnetic Relaxation

None the loss computation methods considered in this paper include relaxation effects [10], [12], [24]. The idea being that if the flux density is quickly ramped to some level and held there, it takes some time for the material internal state to relax to its steady state, and some losses can occur during that relaxation interval. Even if relaxation losses are best (qualitatively and quantitatively) seen for waveforms including

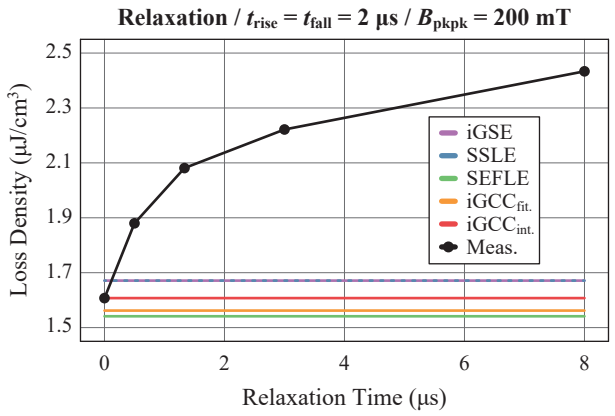

Fig. 11. Energy loss density (per cycle) for symmetric trapezoidal waveforms for different duration of the constant flux density intervals ($t_{\mathrm{cst},1} = t_{\mathrm{cst},2} \in [0, 8]\,\mu\mathrm{s}$). The duration of the two intervals where the flux density is ramped up and down is kept constant ($t_{\mathrm{rise}} = t_{\mathrm{fall}} = 2\,\mu\mathrm{s}$). The peak-to-peak flux density is constant ($B_{\mathrm{pkpk}} = 200\,\mathrm{mT}$). The iGSE, SSLE, SEFLE, and iGCC are compared to measurements.

constant flux density intervals, all waveforms combining fast and slow transients are affected. The fact that the iGCC generally underestimates the losses (see Fig. 8(c)) could be explained by the relaxation losses even if the considered waveforms do not include constant flux density intervals.

Fig. 11 shows the impact of the relaxation losses for symmetric trapezoidal waveforms. The duration of the two intervals where the flux density is ramped up and down is kept constant and the duration of the two intervals where the flux density remains constant is swept. The measured losses are clearly dependent on the duration of the relaxation interval, which is not predicted by the different models. It can be seen that the relaxation effects can increase the losses by more than $50\,\%$. In [10], [13], different methods have been proposed to include the relaxation losses into existing loss models. However, the integration of relaxation mechanisms into the iGCC is outside the scope of this paper.

VII. Conclusion

This paper introduces the iGCC, a core loss model that extends the ISE to arbitrary waveforms. The iGCC decomposes an arbitrary waveform into many symmetric triangular waveforms. Under the CWH, the loss contribution of the decomposed waveforms can be added. The iGCC combines the advantages offered by the ISE (e.g., applicability over a wide frequency range, accuracy with extreme duty cycles, and intuitive interpretation) and the iGSE (e.g., handling of arbitrary waveforms and practicability for design engineers). The disadvantage of the iGCC compared to the iGSE is the model parametrization which requires extensive measurements for symmetric triangular waveforms.

The proposed model has been successfully verified with over ten thousand different measured excitations for "EPCOS TDK N87" material (different frequencies, flux densities, waveforms, and temperatures). The 95$^{\mathrm{th}}$ percentile relative error of the losses predicted by the iGCC is found to be below $13\,\%$, which outperforms the iGSE, SSLE, and SEFLE. Therefore, the iGCC should be preferred whenever enough measurements are available to parametrize the model.

Acknowledgment

This work was supported by ARPA-E under the DIFFERENTIATE program. The research of T. Guillod was supported by the Swiss National Science Foundation (SNSF).

Appendix
Dataset Availability

The "EPCOS TDK N87" datasets used in this paper are part of the MagNet initiative, a joint project between Princeton University, Dartmouth College, and Plexim GmbH [20], [21]. MagNet is an openly available large-scale dataset including measurements of several core materials under various operating conditions.

The datasets used in Section IV and Section V are available for download in [25]. The datasets are proposed in three different formats: CSV files, Python Pandas dataframes (serialized as binary HDF5 files), and MATLAB tables (saved as binary MAT files).

References

[1] J. B. Goodenough, "Summary of Losses in Magnetic Materials," *IEEE Trans. Magn.*, vol. 38, no. 5, pp. 3398–3408, 2002.
[2] P. Thakur, D. Chahar, S. Taneja, N. Bhalla, and A. Thakur, "A Review on MnZn Ferrites: Synthesis, Characterization and Applications," *Ceramics international*, vol. 46, no. 10, p. 15740–15763, 2020.
[3] V. C. Valchev and A. Van den Bossche, *Inductors and Transformers for Power Electronics*. CRC Press, 2005.
[4] J. Reinert, A. Brockmeyer, and R. W. A. A. De Doncker, "Calculation of Losses in Ferro- and Ferrimagnetic Materials Based on the Modified Steinmetz Equation," *IEEE Trans. Ind. Appl.*, vol. 37, no. 4, pp. 1055–1061, 2001.
[5] M. S. Lancarotte and A. de Arruda Penteado, "Estimation of Core Losses under Sinusoidal or Nonsinusoidal Induction by Analysis of Magnetization Rate," *IEEE Trans. Energy Convers.*, vol. 16, no. 2, pp. 174–179, 2001.
[6] K. Venkatachalam, C. R. Sullivan, T. Abdallah, and H. Tacca, "Accurate Prediction of Ferrite Core Loss with Nonsinusoidal Waveforms using only Steinmetz Parameters," in *Proc. of the IEEE Workshop on Computers in Power Electronics*, Jun. 2002.
[7] H. Matsumori, T. Shimizu, T. Kosaka, and N. Matsui, "Core Loss Calculation for Power Electronics Converter Excitation from a Sinusoidal Excited Core Loss Data," *AIP Advances*, vol. 10, no. 4, p. 045001, 2020.
[8] E. Stenglein and T. Dürbaum, "Core Loss Model for Arbitrary Excitations With DC Bias Covering a Wide Frequency Range," *IEEE Trans. Magn.*, vol. 57, no. 6, pp. 1–10, 2021.
[9] C. R. Sullivan and J. H. Harris, "Testing Core Loss for Rectangular Waveforms, Phase II Final Report," PSMA, Tech. Rep., Sep. 2011.
[10] J. Mühlethaler, J. Biela, J. W. Kolar, and A. Ecklebe, "Improved Core-Loss Calculation for Magnetic Components Employed in Power Electronic Systems," *IEEE Trans. Power Electron.*, vol. 27, no. 2, pp. 964–973, 2012.
[11] A. Van den Bossche, V. C. Valchev, and G. B. Georgiev, "Measurement and Loss Model of Ferrites with Non-Sinusoidal Waveforms," in *Proc. of the IEEE Power Electronics Specialists Conf. (PESC)*, Jun. 2004.
[12] C. R. Sullivan, J. H. Harris, and E. Herbert, "Core Loss Predictions for General PWM Waveforms from a Simplified Set of Measured Data," in *Proc. of the IEEE Applied Power Electronics Conf. and Expo. (APEC)*, 2010.
[13] S. Barg, K. Ammous, H. Mejbri, and A. Ammous, "An Improved Empirical Formulation for Magnetic Core Losses Estimation Under Nonsinusoidal Induction," *IEEE Trans. Power Electron.*, vol. 32, no. 3, pp. 2146–2154, 2017.

[14] E. Stenglein, "Messtechnische Charakterisierung und Vorhersage der Kernverluste bei weichmagnetischen Ferriten (in German)," Ph.D. dissertation, Friedrich-Alexander-Universität Erlangen-Nürnberg, Apr. 2021.

[15] E. Stenglein, D. Kübrich, M. Albach, and T. Dürbaum, "Novel Fit Formula for the Calculation of Hysteresis Losses Including DC-Premagnetization," in *Proc. of the Int. Exhib. and Conf. for Power Electronics, Intelligent Motion, Renewable Energy and Energy Management (PCIM Europe),*, May 2019.

[16] J. Mühlethaler, J. Biela, J. W. Kolar, and A. Ecklebe, "Core Losses Under the DC Bias Condition Based on Steinmetz Parameters," *IEEE Trans. Power Electron.*, vol. 27, no. 2, pp. 953–963, 2012.

[17] M. Albach, T. Durbaum, and A. Brockmeyer, "Calculating Core Losses in Transformers for Arbitrary Magnetizing Currents a Comparison of Different Approaches," in *Proc. of the IEEE Power Electronics Specialists Conf. (PESC)*, Jun. 1996.

[18] P. Papamanolis, T. Guillod, F. Krismer, and J. W. Kolar, "Minimum Loss Operation and Optimal Design of High-Frequency Inductors for Defined Core and Litz Wire," *IEEE Open Journal of Power Electronics*, vol. 1, pp. 469–487, 2020.

[19] TDK / EPCOS, "SIFERRIT material N87, Datasheet," 2021. [Online]. Available: https://tdk-electronics.tdk.com

[20] H. Li, D. Serrano, T. Guillod, E. Dogariu, A. Nadler, S. Wang, M. Luo, V. Bansal, Y. Chen, C. R. Sullivan, and M. Chen, "MagNet: An Open-Source Database for Data-Driven Magnetic Core Loss Modeling," in *Proc. of the IEEE Applied Power Electronics Conf. and Expo. (APEC)*, 2022.

[21] Princeton University, Dartmouth College, and Plexim GmbH, "MagNet: Data Driven Methods for Magnetic Core Loss Modeling," 2021. [Online]. Available: https://mag-net.princeton.edu

[22] T. Guillod, "MATLAB Toolbox for Global Fitting/Optimization," 2022. [Online]. Available: https://github.com/otvam/global_optim_fitting_matlab

[23] T. Guillod, "MATLAB Code for Interpolating Triangulated Data," 2021. [Online]. Available: https://github.com/otvam/triangulation_interpolation_matlab

[24] S. Barg and K. Bertilsson, "Core Loss Modeling and Calculation for Trapezoidal Magnetic Flux Density Waveform," *IEEE Trans. Ind. Electron.*, vol. 68, no. 9, pp. 7975–7984, 2021.

[25] T. Guillod, J. S. Lee, H. Li, S. Wang, M. Chen, and C. R. Sullivan, "Calculation of Ferrite Core Losses with Arbitrary Waveforms using the Composite Waveform Hypothesis: Reproducibility Dataset," 2022. [Online]. Available: https://doi.org/10.5281/zenodo.7368936